

Hydrogen-Bonding between Pyrimidine and Water: A Vibrational Spectroscopic Analysis

S. Schlücker,^{*,†} J. Koster,[†] R. K. Singh,[‡] and B. P. Asthana[‡]

Institut für Physikalische Chemie, Universität Würzburg, Am Hubland, 97074 Würzburg, Germany, and Laser and Spectroscopy Laboratory, Department of Physics, Banaras Hindu University, Varanasi – 221005, India

Received: January 11, 2007; In Final Form: March 16, 2007

We present an experimental and a theoretical study on hydrogen-bonding between pyrimidine and water as the H-donor. The degree of hydrogen-bonding in this binary system varies with mixture composition. This was monitored experimentally by polarization-resolved linear Raman spectroscopy with the pyrimidine ring breathing mode ν_1 as a marker band. A subsequent quantitative line shape analysis of the isotropic Raman intensity for 24 pyrimidine/water mixtures clearly revealed a splitting into three spectral components upon dilution with water. The two additional peaks have been assigned to distinct groups of hydrogen-bonded species that differ in the number of pyrimidine nitrogen atoms (N) involved in hydrogen-bonding to water hydrogen atoms (H). From the integrated Raman intensities for “free” and “hydrogen-bonded” pyrimidine, a concentration profile for these species was established. Our assignments and interpretations are supported by quantum mechanical calculations of structures and by vibrational spectra for pyrimidine and 10 pyrimidine/water complexes with increasing water content. Also, accurate structure–spectra correlations for different cluster subgroups have been determined; within each particular cluster subgroup the water content varies, and a perfect negative correlation between NH hydrogen-bond distances and ν_1 wavenumbers was observed.

Introduction

Hydrogen-bonding is an extensively investigated phenomenon,^{1,2} especially due to its importance for biological systems.³ Various experimental methods are employed to characterize hydrogen bonds. For the solid state, NMR spectroscopy is one of the preferred methods.⁴ In the gas phase, vibrational spectroscopy on molecular beams is often performed, which allows one to assess information on isolated hydrogen-bonded complexes.⁵ For the liquid state, where the formation and cleavage of such complexes occurs rapidly, vibrational spectroscopies such as IR and Raman are ideally suited to detect hydrogen-bonding¹ because they cover both structural and dynamic aspects.^{1,6} Whereas the wavenumber position of a vibrational band, which relates to the corresponding internuclear force constants, is dependent on electronic structure and bonding, the line width contains information about molecular dynamics. As compared to IR absorption spectroscopy, Raman spectroscopy can reveal additional information from a line width analysis. Influences on the line width originate, for example, from vibrational relaxation or reorientational motions.^{7,8} These two effects can be separated by applying polarized Raman spectroscopy, where it is possible to determine the pure isotropic part of the Raman scattered intensity (I_{iso}) in which contributions from reorientational motions are absent.⁹ Alternatively, vibrational relaxation dynamics can be directly probed by time-resolved Raman spectroscopy with pico- or femtosecond laser pulses.¹⁰

Pyrimidine is a model structure for the representation of biologically relevant N-heterocycles. In this study, both structural and dynamic aspects of hydrogen-bonding between

pyrimidine and water are investigated experimentally by polarized Raman spectroscopy. This binary model system, which consists of an N-heterocyclic compound with two H-acceptor sites and an H-donor solvent, allows us to continuously monitor the degree of hydrogen-bonding as a function of mixture composition. For a series of pyrimidine/water mixtures, we employ the ring breathing vibration ν_1 of pyrimidine around 990 cm^{-1} as a marker; this vibration is sensitive to hydrogen-bonding between nitrogen-containing heterocycles and H-donor solvents.^{11–16}

The interpretation of vibrational spectroscopic data can be expanded in conjunction with an appropriate theoretical model that correlates the experimentally observed spectral features with explicit molecular structures that are present in the liquid. In this respect, modern quantum chemical approaches can strongly contribute to our understanding of the hydrogen bond.^{17,18} However, two major limitations must be considered. First, particularly accurate electronic structure calculations by rigorous *ab initio* methods are computationally demanding and are presently restricted to small molecular assemblies such as the water dimer.^{19,20} Further, it constitutes a substantive challenge to theoretically describe the molecular dynamics (MD) in a liquid. Several methods for MD simulations have been applied and are continuously improved to reproduce the experimental data available for liquid water;^{21–25} vibrational spectra for liquid water models have, for example, been calculated with Car–Parrinello molecular dynamics (CPMD).²⁶ Also, for solute/solvent mixtures some MD simulations are available; the systems pyridine/water^{27,28} and N-methylacetamide/water²⁴ are mentioned as examples for nitrogen-containing bases dissolved in water. Those studies assume that the hydrogen acceptor molecule is highly diluted, and the quality of the results mainly depends on a correct simulation of both the water environment and the possible hydrogen-bonded solute–water complexes. MD

* To whom correspondence should be addressed. E-mail: sebastian.schluecker@uni-wuerzburg.de

[†] Universität Würzburg.

[‡] Banaras Hindu University.

simulations that consider a variation of the mixture composition and that include high solute concentrations have, however, not been performed so far. For the pyrimidine/water system, only static electronic structure calculations for the isolated 1:1 complex are available.²⁹ This and other studies on hydrogen-bonded 1:1 clusters of N-containing heterocycles and water^{29–33} employed restricted Hartree–Fock (RHF) theory, density functional theory (DFT), and second-order Møller–Plesset (MP2) perturbation theory.

Our vibrational spectroscopic analysis on hydrogen-bonding between pyrimidine and water comprises both experimental Raman spectra and DFT calculations on structures and on vibrational spectra of various pyrimidine/water clusters with increasing water content. We directly relate the computational results to the experimental vibrational wavenumber trends that are observed in our concentration-dependent Raman study.

Methods

Experimental Techniques. Commercially obtained pyrimidine was used without further purification. The parallel (I_{\parallel}) and perpendicular (I_{\perp}) components of the Raman scattered intensity were recorded in the 1030–970 cm^{-1} region for neat pyrimidine and for 24 pyrimidine/water mixtures with mole fractions of pyrimidine ranging from $x(\text{pd}) = 0.02$ to 1.00. The 514.5 nm line of an Ar^+ laser that delivered ~ 100 mW power to the sample was used for excitation; the signal was collected in a 90° scattering geometry. A double monochromator (Spex 1404) with 2400 grooves/mm gratings and a liquid N_2 -cooled charge-coupled device (CCD) detector (Photometrics) were employed to record the Raman spectra. The high spectral resolution of ~ 0.36 cm^{-1} , equivalent to an entrance slit width of 50 μm , allows for the determination of peak positions and of line widths with high accuracy. For all measurements, the grating position was kept constant, which ensures a high precision and reproducibility of peak positions. The I_{\parallel} and I_{\perp} components of the Raman scattered intensity were measured for each binary mixture by turning the polarization of the incident laser beam by 90° using a double Fresnel rhomb before the sample; the analyzer position was kept constant to avoid errors due to the polarization dependency of the detection system.

Computational Methods. Electronic structure calculations on pyrimidine and on various hydrogen-bonded complexes of pyrimidine and water were carried out using DFT. Geometry optimizations and calculations of vibrational spectra were performed using the GAUSSIAN98 (Rev. A7) suite of programs employing tight convergence criteria. The B3LYP hybrid functional and the 6-31++G(d,p) basis set were employed. Internal coordinates were generated using the MOLDEN program (Version 3.4), by starting from pyrimidine and then successively adding water molecules.

Results and Discussion

DFT Calculations on Pyrimidine/Water Complexes. In the binary pyrimidine/water system, many different hydrogen-bonded complexes can be simultaneously present. The two nitrogen atoms of pyrimidine (Pd) are potential hydrogen-acceptor sites; additionally, each water (W) molecule offers two hydrogen-bond acceptor and two donor sites. We therefore calculated the structures and the vibrational spectra of various small Pd_xW_y clusters with stoichiometric ratios $x:y$ ranging from 2:1 to 1:6.

Structures and $\text{N}\cdots\text{H}$ Bond Distances. The structures of the 2:1 (Pd_2W) to 1:3 (PdW_3) clusters are shown in Figure 1. In the 2:1 (Pd_2W) complex, the two Pd rings are symmetrically

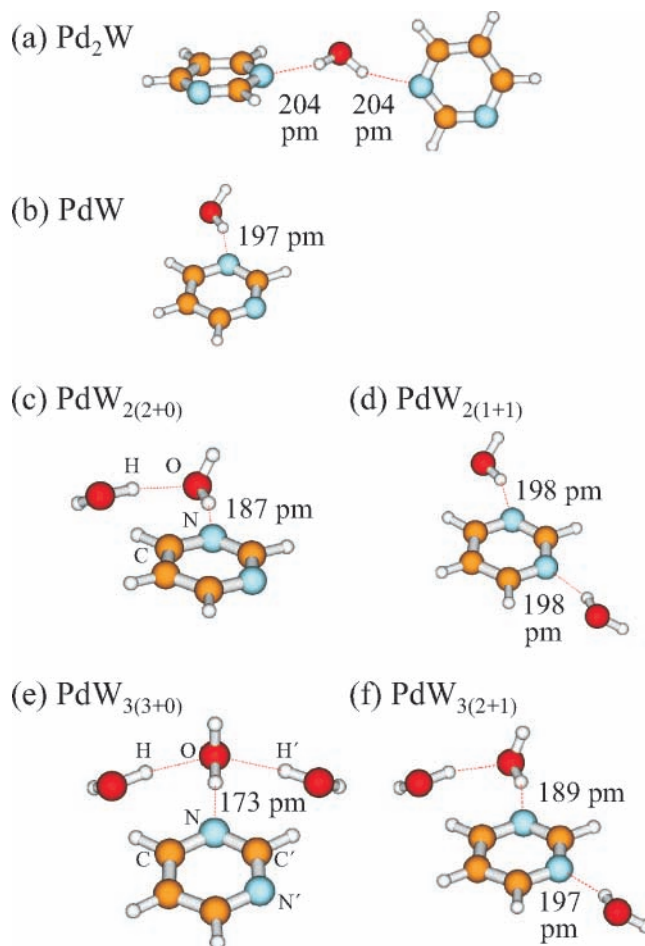


Figure 1. (a–f) Optimized geometries of various hydrogen-bonded Pd_xW_y complexes (Pd_xW_y) with different stoichiometric ratios $x:y$ reaching from 2:1 to 1:3. The DFT calculated $\text{N}\cdots\text{H}$ distances are indicated.

connected by hydrogen bonds to the water molecule (Figure 1a). The perpendicular orientation of the aromatic rings is attributed to the minimization of repulsive π – π interactions between the two Pds. Similarly, the relative orientation of water results from minimized interactions between the oxygen lone pairs and the two π -electron systems. Both $\text{N}\cdots\text{H}$ hydrogen-bond distances are 204 pm, which is the largest calculated value within this series of Pd_xW_y clusters. The 1:1 (PdW) complex depicted in Figure 1b exhibits a shorter $\text{N}\cdots\text{H}$ bond length and a more linear $\text{N}\cdots\text{H}$ –O bond angle as compared with the 2:1 (Pd_2W) complex, which indicates the formation of a stronger hydrogen bond.

Hydrogen-bonding of two water molecules to Pd may lead to complexes such as the $\text{PdW}_{2(2+0)}$ or the $\text{PdW}_{2(1+1)}$ clusters shown in Figure 1, panels c and d, respectively. In the $\text{PdW}_{2(2+0)}$ complex (Figure 1c), the $\text{N}\cdots\text{H}$ bond length of 187 pm is shorter as compared to 197 pm for the 1:1 (PdW) species (Figure 1b); the orientation of the $\text{O}\cdots\text{H}$ hydrogen bond between the two water molecules is practically coplanar with the Pd ring plane: the calculated dihedral angle C–N O \cdots H is 1° . In contrast to the $\text{PdW}_{2(2+0)}$ species, the $\text{PdW}_{2(1+1)}$ cluster (Figure 1d), in which Pd is nearly C_2 symmetrically complexed by two water molecules, reveals an $\text{N}\cdots\text{H}$ bond length of 198 pm for both hydrogen-bonding sites. This indicates that the strength of each hydrogen bond in $\text{PdW}_{2(1+1)}$ is close to that in the 1:1 (PdW) complex.

Similar to the 1:2 stoichiometry, hydrogen-bonding of three water molecules to Pd can result in the formation of the two

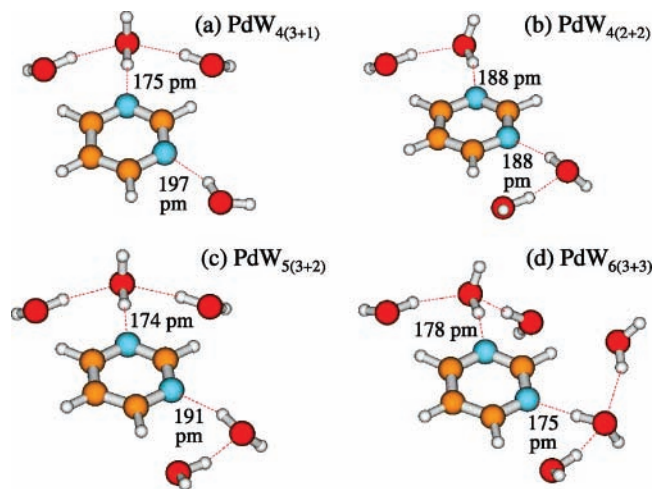


Figure 2. (a–d) Optimized geometries of various hydrogen-bonded Pd/W complexes (Pd_xW_y) with different stoichiometric ratios $x:y$ reaching from 1:4 to 1:6. The DFT calculated $\text{N}\cdots\text{H}$ distances are indicated.

PdW_3 clusters depicted in Figure 1, panels e and f. In the $\text{PdW}_{3(3+0)}$ complex (Figure 1e), the arrangement of all three water molecules in a single W_3 subcluster causes a significant $\text{N}\cdots\text{H}$ bond contraction to 173 pm as compared to 186 pm for $\text{PdW}_{2(2+0)}$ (Figure 1c). The orientation of the two outer water molecules to the central $\text{N}\cdots\text{H}$ bonded water in $\text{PdW}_{3(3+0)}$ is not symmetrical: the dihedral angles $\text{C}-\text{N}\cdots\text{O}\cdots\text{H}$ and $\text{C}'-\text{N}\cdots\text{O}\cdots\text{H}'$ are -120° and 16° , respectively. This also implies that the $\text{O}\cdots\text{H}$ bonds are not coplanar relative to the molecular plane of Pd as in the $\text{PdW}_{2(2+0)}$ complex (Figure 1c). Apart from the $\text{PdW}_{3(3+0)}$ species, a $\text{PdW}_{3(2+1)}$ complex can be formed by adding a third water molecule to the $\text{PdW}_{2(1+1)}$ cluster; in the $\text{PdW}_{3(2+1)}$ complex (Figure 1f), only the $\text{N}\cdots\text{H}$ bond of that water molecule, which is hydrogen-bonded to a second water, is shortened to 189 pm as compared with 198 pm for $\text{PdW}_{2(1+1)}$ (Figure 1d). Similar to the $\text{PdW}_{3(3+0)}$ species (Figure 1c), the $\text{C}-\text{N}\cdots\text{O}\cdots\text{H}$ dihedral angle is 0° ; that is, the OH bond is coplanar with the molecular plane of Pd.

The structures of various 1:4 (PdW_4), 1:5 (PdW_5), and 1:6 (PdW_6) clusters are shown in Figure 2. Our analysis is restricted to species with a maximum of three water molecules (W_3 subclusters) attached to each nitrogen atom of Pd. From a calculation on PdW_4 (results not shown), we consider the effect of a fourth water molecule on both the $\text{N}\cdots\text{H}$ distance and the vibrational wavenumber of ν_1 to be negligible. In contrast, as described in the previous paragraph, the addition of a second and a third water molecule induces a recognizable strengthening of the corresponding $\text{N}\cdots\text{H}$ hydrogen bond; this becomes clear, for example, by comparing the complexes $\text{PdW}_{2(1+1)}$ (Figure 1d), $\text{PdW}_{4(2+2)}$ (Figure 2b), and $\text{PdW}_{6(3+3)}$ (Figure 2d): both $\text{N}\cdots\text{H}$ bonds are shortened by about 10 pm upon the addition of each new sphere of water molecules. In $\text{PdW}_{4(2+2)}$ as well as in $\text{PdW}_{6(3+3)}$ the dihedral angles $\text{C}-\text{N}\cdots\text{O}\cdots\text{H}$ and $\text{C}'-\text{N}'\cdots\text{O}\cdots\text{H}'$ indicate coplanar $\text{O}\cdots\text{H}$ orientations.

The $\text{PdW}_{5(3+2)}$ complex depicted in Figure 2c exhibits a 174 pm $\text{N}\cdots\text{H}$ bond to the W_3 subcluster and a longer 191 pm $\text{N}\cdots\text{H}$ bridge to the W_2 subcluster. In comparison to the $\text{PdW}_{4(3+1)}$ species in Figure 2a, the addition of the fifth water molecule introduces a $\text{N}\cdots\text{H}$ bond contraction from 197 to 191 pm in $\text{PdW}_{5(3+2)}$; the same effect on the shorter $\text{N}\cdots\text{H}$ bond is negligible (175 to 174 pm). The orientation of the two outer water molecules in the W_3 subcluster of $\text{PdW}_{5(3+2)}$, however, is more symmetrical as compared with the $\text{PdW}_{3(3+0)}$ species

TABLE 1: $\text{N}\cdots\text{H}$ Bond Distances and ν_1 Wavenumbers for Pure Pd and Various Hydrogen-Bonded Pd_xW_y Complexes^a

complex	$d(\text{N}\cdots\text{H})$ (pm)	$d(\text{N}'\cdots\text{H})$ (pm)	$\tilde{\nu}_1$ (cm^{-1})
Pd			1012
Pd_2W	204/204		1018
PdW	197		1020
$\text{PdW}_{2(2+0)}$	187		1022
$\text{PdW}_{2(1+1)}$	198	198	1027
$\text{PdW}_{3(3+0)}$	173		1026
$\text{PdW}_{3(2+1)}$	189	197	1029
$\text{PdW}_{4(3+1)}$	175	197	1032
$\text{PdW}_{4(2+2)}$	188	188	1031
$\text{PdW}_{5(3+2)}$	174	191	1035
$\text{PdW}_{6(3+3)}$	178	175	1038

^a Calculated using DFT at the B3LYP/6-31++G(d,p) level.

in Figure 1e: the dihedral angles $\text{C}-\text{N}\cdots\text{O}\cdots\text{H}$ and $\text{C}'-\text{N}\cdots\text{O}\cdots\text{H}'$ are -14° and 14° , respectively.

Upon further water addition to $\text{PdW}_{5(3+2)}$, a second W_3 subcluster is formed; the structure of the corresponding $\text{PdW}_{6(3+3)}$ cluster is depicted in Figure 2d. In contrast to the nearly C_2 symmetric $\text{PdW}_{2(1+1)}$ and $\text{PdW}_{4(2+2)}$ complexes in Figures 1d and 2b, respectively, the $\text{N}\cdots\text{H}$ bond lengths of 178 and 175 pm are not equivalent and large deviations from an overall C_2 symmetry are noted. We hypothesize that the asymmetry observed for $\text{PdW}_{6(3+3)}$ is induced by the repulsive interactions between the two W_3 subclusters. The through-space distance between the oxygen atoms of the two closest water molecules (top right) is 573 pm. The corresponding $\text{N}\cdots\text{H}$ distances for all Pd_xW_y clusters depicted in Figures 1 and 2 are summarized in Table 1.

Wavenumber Shifts of the Pd Ring Breathing Mode upon Complexation. In this study, the Raman peak position of the Pd ring breathing mode ν_1 serves as a probe for monitoring the degree of hydrogen-bonding between Pd and water. We therefore calculated the vibrational spectra of all Pd_xW_y clusters from Figures 1 and 2. The corresponding harmonic and unscaled wavenumber values for $\tilde{\nu}_1(\text{pd})$ are listed in Table 1. The values for $\tilde{\nu}_1(\text{pd})$ extend over a range of 20 cm^{-1} and increase from 1018 cm^{-1} for Pd_2W to 1038 cm^{-1} for $\text{PdW}_{6(3+3)}$. At first glance, one may assume a positive correlation of $\tilde{\nu}_1(\text{pd})$ with the Pd/W stoichiometry (2.0 for Pd_2W to 0.17 for PdW_6); the different $\tilde{\nu}_1(\text{pd})$ values for clusters with the same stoichiometric Pd/W ratio (e.g., 1026 cm^{-1} for $\text{PdW}_{3(3+1)}$ vs 1029 cm^{-1} for $\text{PdW}_{3(2+1)}$) indicate, however, that this is apparently not the case. Similarly, it is difficult to identify a general correlation of the $\text{N}\cdots\text{H}$ bond distances with $\tilde{\nu}_1(\text{pd})$ for the entire series.

We identified, however, perfect negative correlations (regression coefficients $R > 0.999$) between the $\text{N}\cdots\text{H}$ bond distance and $\tilde{\nu}_1(\text{pd})$ for certain subgroups of Pd_xW_y clusters. Figure 3 (bottom) demonstrates this for the “ $x + 0$ ” series, which consists of Pd_2W , PdW , $\text{PdW}_{2(2+0)}$, and $\text{PdW}_{3(3+0)}$: for each cluster within this subgroup, only one nitrogen per Pd molecule is involved in hydrogen-bonding. Figure 3 (middle) displays the corresponding negative correlation for the “ $x + 1$ ” series with $\text{PdW}_{2(1+1)}$, $\text{PdW}_{3(2+1)}$, and $\text{PdW}_{4(3+1)}$: within this series, one Pd nitrogen is already complexed with one water ($\text{N}\cdots\text{H}$ ca. 197–198 pm), and additional water molecules are successively added to the second nitrogen. The regression lines for these two subgroups are separated by approximately 7 cm^{-1} , and their slopes are very similar with $-0.262\text{ cm}^{-1}/\text{pm}$ for the $x + 0$ series and $-0.236\text{ cm}^{-1}/\text{pm}$ for the $x + 1$ series, respectively; this indicates that the wavenumber shifts induced by water complexation are comparable for both subgroups. A similar behavior is observed for the “ $x + 2$ ” series (Figure 3, top).

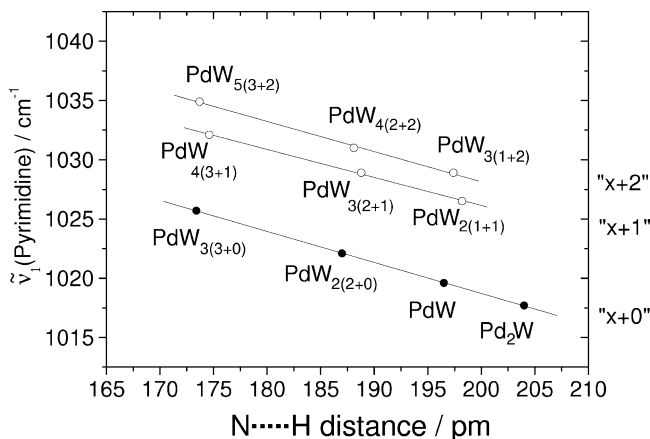


Figure 3. Correlation of calculated ν_1 wavenumbers and calculated $N\cdots H$ distances. Linear correlations are displayed for three groups of Pd/W complexes, where one Pd binding site is non-hydrogen-bonded ($x + 0$) or coordinated to either one ($x + 1$) or two ($x + 2$) water molecules.

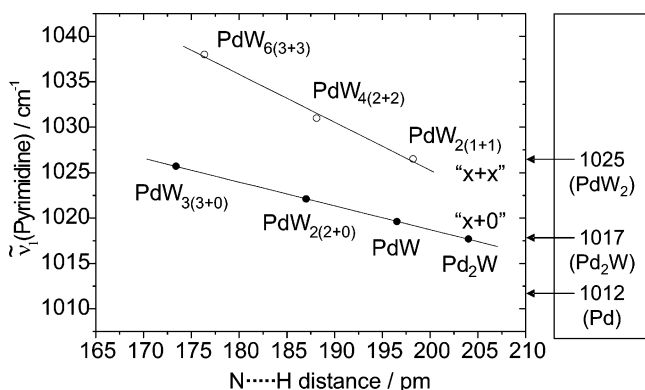


Figure 4. Correlation of calculated ν_1 wavenumbers and calculated $N\cdots H$ distances. Linear correlations are displayed for a series of complexes where only one Pd binding site or both Pd binding sites are successively complexed by water molecules ($x + 0$ and $x + x$ series). The calculated wavenumbers (in cm^{-1}) for the complexes with lowest water content of these series ($\text{PdW}_{2(1+1)}$ and Pd_2W) are indicated together with the calculated wavenumber for free Pd.

The effect of adding two water molecules, one to each nitrogen atom of Pd, is illustrated in Figure 4. This subgroup is labeled “ $x + x$ ” and contains the complexes $\text{PdW}_{2(1+1)}$, $\text{PdW}_{4(2+2)}$, and $\text{PdW}_{6(3+3)}$. The slope of the regression line for the $x + x$ series is two times larger as compared with the subgroups in which only one molecule of water is successively added; the regression line for the $x + 0$ series is shown for comparison in Figure 4. This suggests that simultaneously adding two water molecules instead of one doubles the induced wavenumber shift. In addition to the hydrogen-bonded species, the noncomplexed or “free” Pd must be considered. The calculated wavenumber of ν_1 for this isolated Pd is 1012 cm^{-1} as indicated in Figure 4 (right bottom). Hence, free Pd is clearly spectrally separated from all hydrogen-bonded subgroups; the difference to the lowest wavenumber of the $x + 1$ series is 5 cm^{-1} .

Our calculations lead to two major assumptions for Raman experiments on Pd/W mixtures. First, the resolution of different hydrogen-bonded species seems possible because of obvious wavenumber differences; second, shifts of ν_1 toward higher wavenumbers are expected with increasing water content. Therefore, concentration-dependent Raman spectra, covering the ring breathing mode ν_1 of Pd, should be capable of monitoring the degree of hydrogen-bonding between Pd and W.

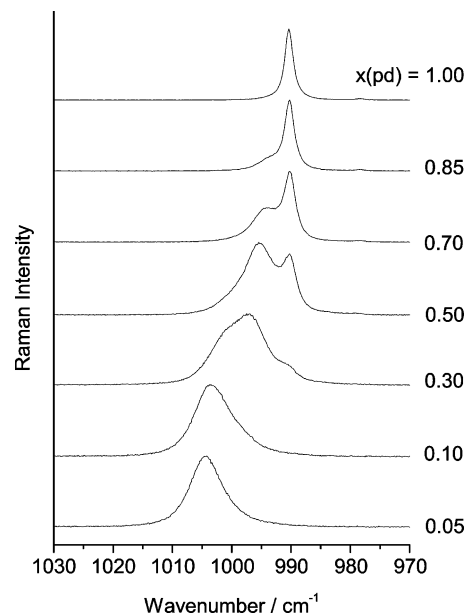


Figure 5. Isotropic components of the Raman spectra of Pd/W mixtures for selected mixture compositions; $x(\text{pd})$ indicates the Pd mole fraction.

Polarization-Resolved Raman Spectroscopy. Polarization-resolved linear Raman spectra of neat Pd and of 24 binary Pd/W mixtures with mole fractions of Pd ranging from $x(\text{pd}) = 1.00$ to 0.02 were recorded in the wavenumber interval $1030\text{--}960 \text{ cm}^{-1}$. The isotropic components (I_{iso}) of the Raman spectra were determined by use of a linear combination of spectra recorded with I_{\parallel} and I_{\perp} .^{6,9}

$$I_{\text{iso}} = I_{\parallel} - \frac{4}{3}I_{\perp} \quad (1)$$

For seven selected Pd mole fractions, the isotropic components in the wavenumber range $1030\text{--}960 \text{ cm}^{-1}$ are shown in Figure 5. Neat Pd (Figure 5, top) shows a band at $\approx 990 \text{ cm}^{-1}$, which is assigned to the ring breathing mode ν_1 ; its ^{13}C satellite is observed as a weak band at $\approx 978 \text{ cm}^{-1}$. Upon the addition of water, the appearance of a new band at $\approx 994 \text{ cm}^{-1}$ is observed ($x(\text{pd}) = 0.96$, not shown). It is assigned to the ring breathing mode ν_1 of hydrogen-bonded Pd. As can be seen from the Raman spectra for $x(\text{pd}) = 0.85$ and 0.70 in Figure 5, both the relative intensity and the wavenumber value of this additional Raman band increase. For $x(\text{pd}) = 0.50$ and 0.30 , a qualitative analysis of the band envelope suggests the presence of three distinct spectral components for intermediate dilutions. At very high dilutions, i.e., $x(\text{pd}) = 0.10$ and 0.05 (Figure 5, bottom), only contributions of hydrogen-bonded species are observed.

Decomposition of Isotropic Raman Components. To quantify this trend for the concentration-dependent isotropic Raman spectra, a decomposition of the band envelope for each mixture composition was performed. This is shown exemplarily in Figure 6 for Pd mole fractions $x(\text{pd}) = 0.85$, 0.50 , and 0.10 , which represents low, intermediate, and high dilutions, respectively, of Pd with water. For mole fractions $x(\text{pd}) = 0.96$ to 0.85 , the overall band profile was fitted to two Voigt profiles, which reflects the presence of chemically distinct species consisting of hydrogen-bonded and non-hydrogen-bonded or free Pd, respectively. At $x(\text{pd}) = 0.82$ (not shown), a weak third band at $\approx 999 \text{ cm}^{-1}$ is observed in the Raman spectrum. According to the higher wavenumber value of $\approx 999 \text{ cm}^{-1}$ as compared to $\approx 994 \text{ cm}^{-1}$ for the second band, it is assigned to ν_1 of Pd present in hydrogen-bonded complexes with a larger

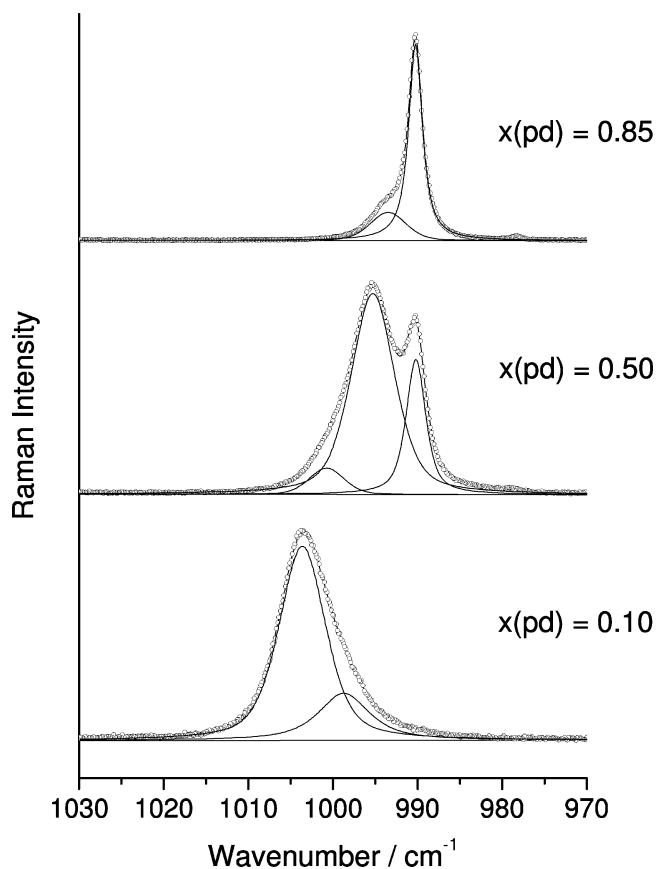


Figure 6. Isotropic components of the Raman spectra (circles) of Pd/W mixtures for selected mixture compositions; $x(\text{pd})$ indicates the Pd mole fraction. Also shown are the corresponding spectra together with single band contributions (lines) resulting from a least-squares curve fit assuming two (for $x(\text{pd}) = 0.85$ and 0.10) or three (for $x(\text{pd}) = 0.50$) Voigt-shaped bands, respectively.

overall water content. Three Voigt profiles were employed to fit the spectra recorded for mole fractions $x(\text{pd})$ from 0.82 to 0.13. The isotropic part of the Raman spectrum for $x(\text{pd}) = 0.50$ shown exemplarily in Figure 6 clearly exhibits the presence of two hydrogen-bonded and a single non-hydrogen-bonded Pd species. The corresponding band positions and their integrated intensity ratios or relative concentrations vary as a function of the mixture composition. For mole fractions $x(\text{pd}) = 0.10$ and below, the amount of non-hydrogen-bonded or free Pd is almost negligible and two Voigt profiles were considered to be sufficient to reflect the observed spectral characteristics.

Finally, it is noted that the corresponding anisotropic components of the Raman spectra show the same systematic trends (see Supporting Information).

Concentration Profile of Free Pyrimidine and Hydrogen-Bonded Species. To obtain a more detailed picture of the relative concentration of different Pd species, the band area ratios of the fitted Voigt profiles were analyzed. It is to be noted that this approach is based on two assumptions: (1) the Raman scattering cross sections of free Pd and of the various hydrogen-bonded Pd species are comparable, and (2) the cross section for each species is constant over the examined mole fraction range.

The concentration profiles for free Pd(pd) and for the two distinct groups of hydrogen-bonded species (pd1 and pd2) as derived from integrated intensity ratios are presented in Figure 7. In the mole fraction range from 1.0 to 0.4, the relative concentration of free Pd decreases linearly to below 20%. Upon

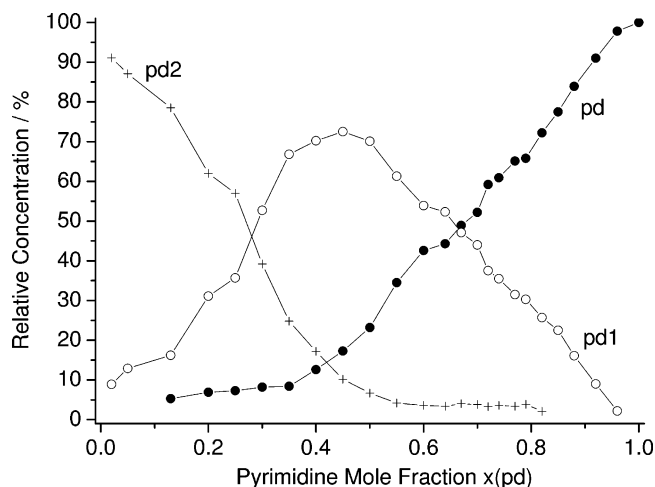


Figure 7. Concentration profiles of the three spectrally identified Pd species pd, pd1, and pd2; relative concentrations are derived from Raman band area ratios.

further dilution the concentration also decreases linearly, but with a significantly smaller slope, to about 5% at $x(\text{pd}) = 0.13$.

The concentration profile for Pd in hydrogen-bonded complexes with a low water content (pd1) is also shown in Figure 7. Upon the initial addition of water, starting at $x(\text{pd}) = 0.96$, the concentration of this hydrogen-bonded Pd species increases linearly to about 70% at $x(\text{pd}) = 0.50$. The absolute value of the slope is slightly smaller as compared to the decrease of free Pd. This is attributed to the formation of the second hydrogen-bonded species (pd2) with a larger water content as compared to pd1. After reaching a maximum concentration of approximately 73% at $x(\text{pd}) = 0.45$, the pd1 species concentration decreases rapidly upon further dilution and approaches less than 9% for the lowest recorded mole fraction of $x(\text{pd}) = 0.02$. The concentration for pd2 remains nearly constant at low levels (2–4%) over the mole fraction range 0.82–0.55. Upon further dilution, the concentration increases rapidly and reaches 91% at $x(\text{pd}) = 0.02$.

The concentration profile may be understood in terms of mechanisms of formation of pd1 and pd2. As water is initially added to the Pd, up to $x(\text{pd}) = 0.45$, the mole fractions of Pd and water are such that formation of only pd1 complexes, apart from free Pd, takes place. Only a very small fraction of water molecules is involved in forming pd2 complexes; the relative pd2 concentration remains at low levels of 2–4% up to $x(\text{pd}) = 0.55$. This essentially means that at about $x(\text{pd}) = 0.5$, an equilibrium between the concentrations of free Pd molecules and the pd1 species is reached. Upon further dilution, both free Pd molecules and those from pd1 complexes are rapidly consumed to form the pd2 species. At higher dilutions, below $x(\text{pd}) \approx 0.5$, the relative pd2 concentration increases rapidly and reaches up to ~90% at $x(\text{pd}) = 0.02$. Correspondingly, the pd1 concentration decreases and approaches ~10% at $x(\text{pd}) = 0.02$.

In addition to the construction of a concentration profile, our quantitative band decomposition also allows a separate analysis of the concentration dependence of wavenumbers and line widths for each species.

Wavenumber Shift and Line Width Analysis. Both wavenumber values and line widths (full width at half-maximum: FWHM) of the ring breathing mode ν_1 of Pd present in the three kinds of species (pd, pd1, pd2) depend on the mixture composition as shown in Figures 8 and 9. Our interpretation of the observed concentration dependence of ν_1 in a particular

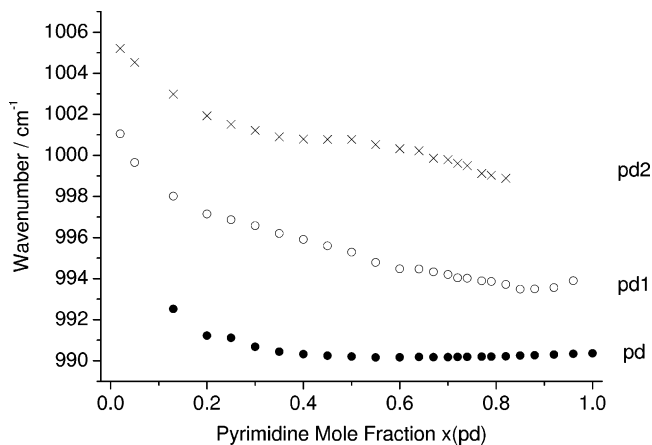


Figure 8. Concentration dependence of the ν_1 wavenumber for the three Pd species pd, pd1, and pd2.

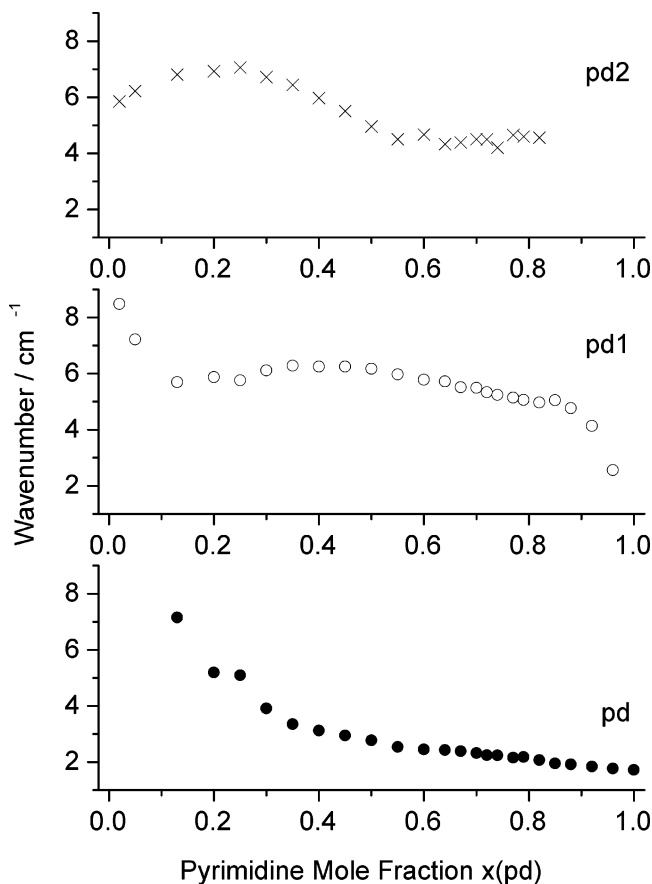


Figure 9. Concentration dependence of the ν_1 line width for the three Pd species pd, pd1, and pd2.

species is based on the assumption that this mode probes the chemical composition of the species and, to a certain extent, the interaction with its environment. In addition, the analysis of the concentration dependence of the line width is capable of probing dynamic processes such as concentration fluctuations within certain species and diffusion of the solvent water into the reference system Pd.^{6,34}

Non-Hydrogen-Bonded or Free Pd. For non-hydrogen-bonded or free Pd, the wavenumber of $\nu_1(\text{pd})$ exhibits a small shift to smaller wavenumbers upon the addition of water as shown in Figure 8 (bottom). This negative shift is linear, starting from neat Pd to about $x(\text{pd}) = 0.80$. In the mole fraction range from 0.80 to 0.55, the decrease of $\nu_1(\text{pd})$ becomes still smaller; the minimum value of $\nu_1(\text{pd})$ at $x(\text{pd}) = 0.55$ lies only 0.2 cm^{-1}

below that of neat Pd. The further addition of water causes a rapid increase of $\nu_1(\text{pd})$; at $x(\text{pd}) = 0.13$, the highest dilution for which free Pd could be detected, it finally approaches 992.5 cm^{-1} . A comparison with the concentration profiles depicted in Figure 7 shows that within the mole fraction range of 1.00–0.60, the concentration of pd decreases to below 50%, and the pd1 species concentration increases to above 50%. The observed small negative wavenumber shift of ν_1 is attributed to the increased interaction between pd and its environment; we assume that either the hydrogen-bonded species or water clusters induce a very small reduction of the electron density of the pd ring, which causes a slightly smaller force constant and wavenumber for the ν_1 vibration, respectively. This assumption is supported by the observation that, as shown in Figure 9 (bottom), the line width of $\nu_1(\text{pd})$ increases linearly from 1.7 to 2.5 cm^{-1} in the range $x(\text{pd}) = 1.0$ –0.55; this line broadening indicates that the pd molecules are present in a larger number of microstates and that, due to the larger interaction with the surroundings, vibrational dephasing of this mode occurs faster. The drastic increase in both wavenumber position and line width for high dilutions is explained in terms of diffusion of water molecules into the reference system Pd; the wavenumber position of $\nu_1(\text{pd})$ approaches a value close to that observed for the pd1 species at very low dilutions (see Figure 8), indicating that Pd molecules in the pd system are involved in weak hydrogen-bonding.

Hydrogen-Bonded Pd Species with Low Water Content. The concentration dependence of the wavenumber position for $\nu_1(\text{pd1})$ in the hydrogen-bonded species pd1 shown in Figure 8 (center) is similar to that of free Pd depicted in Figure 8 (bottom). In the mole fraction range from $x(\text{pd}) = 0.96$ to 0.85, $\nu_1(\text{pd1})$ also exhibits a slight shift to smaller wavenumber values by about 0.5 cm^{-1} . Similar to the explanation for free Pd, this is attributed to the impact of water clusters in proximity to the pd1 complexes, withdrawing electron density from the pd ring system. This assumption is supported by the corresponding line width data in Figure 9 (center), which reveal a significant degree of line broadening by almost a factor of 2 from 2.6 cm^{-1} at $x(\text{pd}) = 0.96$ to 5.1 cm^{-1} at $x(\text{pd}) = 0.85$. The wavenumber data for $\nu_1(\text{pd1})$ show a linear increase over the large mole fraction range of 0.80–0.20, which shows that the water content in this hydrogen-bonded species is constantly growing. The corresponding line width data resemble a Gaussian-like profile, which is characteristic of the phenomenon of concentration fluctuations.³⁴ The plateau between $x(\text{pd}) = 0.50$ and 0.35 indicates that for these mixture compositions the largest concentration fluctuations, that is, variations in the local concentration by exchanging neighbors with various composition, occur. Similar to free Pd, both the ν_1 wavenumber and the line width increase rapidly for high dilutions. For $x(\text{pd}) = 0.02$, the wavenumber value of $\approx 1001 \text{ cm}^{-1}$ shows that the degree of hydrogen-bonding has significantly increased; from this observation we conclude that the average composition involves multiple hydrogen-bonded pd1 species, which is similar to the situation in the pd2 species.

Hydrogen-Bonded Pd Species with High Water Content. The concentration dependence of the wavenumber position for $\nu_1(\text{pd2})$ in the hydrogen-bonded species pd2 shown in Figure 8 (top) exhibits a slightly different behavior as compared with the concentration profiles for the pd and pd1 species in Figure 8 (bottom and center, respectively). At $x(\text{pd}) = 0.82$, the first mixture for which the pd2 species is detectable upon the addition of water, the wavenumber value for $\nu_1(\text{pd2})$ is $\approx 999 \text{ cm}^{-1}$. In the mole fraction range $x(\text{pd}) = 0.82$ –0.55, a

linear increase in the $\nu_1(\text{pd}2)$ wavenumber position is observed (see Figure 8); this shows that the overall water content and, correspondingly, that the degree of hydrogen-bonding in terms of multiple hydrogen-bonded Pd molecules in this species is growing. In this concentration interval, the relative pd2 concentration remains below 5% (see Figure 7). The corresponding line widths shown in Figure 9 (top) are constant within $\pm 0.25 \text{ cm}^{-1}$ and, therefore, do not suggest the diffusion of water into the pd2 system. In combination with the wavenumber and the line width profiles obtained for the pd1 species, a possible explanation might be that the primary source for the observed increasing water content in the pd2 system are pd1 species; the pd1 complexes themselves might recruit water molecules from water clusters as discussed above. In the mole fraction range $x(\text{pd}) = 0.55\text{--}0.40$, the wavenumber profile in Figure 8 (top) exhibits a plateau, which indicates that the chemical composition of the hydrogen-bonded pd2 system remains constant. The relative concentration of the pd2 complexes, however, increases from $\approx 4\%$ to $> 17\%$ as shown in the corresponding concentration profile in Figure 7. At the same time, the line width data depicted in Figure 9 (top) indicate that diffusion of water molecules into the pd2 system occurs. As a possible explanation for this complex behavior, we suggest that the relative concentration of the pd2 species increases by diffusion of either hydrogen-bonded Pd or water molecules into the pd2 system, which leaves the average extent of hydrogen-bonding nearly constant; this explanation would cover both the observed wavenumber and the line width profiles. Upon further dilution, the wavenumber of $\nu_1(\text{pd}2)$ increases rapidly up to $\approx 1005 \text{ cm}^{-1}$ at $x(\text{pd}) = 0.02$, which reveals the presence of a large amount of multiple hydrogen-bonded Pd molecules within this species. The line width profile in Figure 9 (top) exhibits, similar to the hydrogen-bonded pd1 species, the phenomenon of concentration fluctuations. The maximum line width is observed for $x(\text{pd}) = 0.25$ or a Pd/W ratio of 1:3; this indicates, in addition to the wavenumber data, that multiple rather than single hydrogen-bonded pd2 species are formed.

Conclusions

Binary mixtures of Pd and water are a complex molecular system that comprises non-hydrogen-bonded and various hydrogen-bonded species. The quantitative analysis of our experimental Raman spectra demonstrates that both their relative concentrations and their dynamic exchange is dependent upon the composition of the mixture. The presented quantum mechanical calculations on Pd/W clusters with varying water content and single or multiple hydrogen bonds suggest that they can be differentiated by high-resolution gas-phase vibrational spectroscopy. Probing these individual hydrogen-bonded species in the liquid state may be achieved by single molecule vibrational spectroscopy, for example, by surface-enhanced Raman scattering (SERS). Increased computational resources will make high-level molecular dynamics simulations of complex hydrogen-bonded mixtures feasible. For the Pd/W system, our DFT derived structures and vibrational spectra may serve as a starting point for ab initio MD or CPMD simulations. The reliability of these calculations can be tested by comparison with our experimental Raman spectra: the statistical distribution of all individual species weighted with their relative contributions must reflect the intrinsic Raman band envelope.

Acknowledgment. Financial support from the German Research Foundation (DFG, SFB 630, TP C1), the Alexander-von-Humboldt (AvH) foundation, and the German Academic Exchange Service (DAAD) is highly acknowledged. SS thanks Prof. Wolfgang Kiefer, Universität Würzburg, for access to laser spectroscopic facilities.

Supporting Information Available: Anisotropic components of the Raman spectra at various Pd/W ratios. This material is available free of charge via the Internet at <http://pubs.acs.org>.

References and Notes

- (1) Pimentel, G. C.; McClellan, A. L. *The Hydrogen Bond*; Freeman: San Francisco, 1960.
- (2) Perrin, C. L.; Nielson, J. B. *Annu. Rev. Phys. Chem.* **1997**, *48*, 511.
- (3) Jeffrey, G. A.; Saenger, W. *Hydrogen Bonding in Biological Structures*; Springer: Berlin, 1991.
- (4) Schlund, S.; Mladenovic, M.; Basilio Janke, E. M.; Engels, B.; Weisz, K. *J. Am. Chem. Soc.* **2005**, *127*, 16151.
- (5) Andrei, H.-S.; Solcà, N.; Dopfer, O. *ChemPhysChem* **2006**, *7*, 107.
- (6) Asthana, B. P.; Kiefer, W. In *Vibrational Spectra and Structure*; Durig, J. R., Ed.; Elsevier: Amsterdam, 1992; Vol. 20, p 67.
- (7) Gordon, R. G. *J. Chem. Phys.* **1965**, *43*, 1307.
- (8) Rothschild, W. G. *Dynamics of Molecular Liquids*; Wiley: New York, 1983.
- (9) Bartoli, F. J.; Litovitz, T. A. *J. Chem. Phys.* **1972**, *56*, 413.
- (10) Laubereau, A.; Kaiser, W. *Rev. Mod. Phys.* **1978**, *50*, 607.
- (11) Takahashi, H.; Mamola, K.; Plyler, E. K. *J. Mol. Spectrosc.* **1966**, *21*, 217.
- (12) Asthana, B. P.; Takahashi, H.; Kiefer, W. *Chem. Phys. Lett.* **1983**, *94*, 41.
- (13) Deckert, V.; Asthana, B. P.; Mishra, P. C.; Kiefer, W. *J. Raman Spectrosc.* **1996**, *27*, 907.
- (14) Schlücker, S.; Singh, R. K.; Asthana, B. P.; Popp, J.; Kiefer, W. *J. Phys. Chem. A* **2001**, *105*, 9983.
- (15) Schlücker, S.; Heid, M.; Singh, R. K.; Asthana, B. P.; Popp, J.; Kiefer, W. *Z. Phys. Chem.* **2002**, *216*, 267.
- (16) Berg, E. R.; Freeman, S. A.; Green, D. D.; Ulness, D. J. *J. Phys. Chem. A* **2006**, *110*, 13434.
- (17) Gordon, M. S.; Jensen, J. H. *Acc. Chem. Res.* **1996**, *29*, 536.
- (18) Schlund, S.; Schmuck, C.; Engels, B. *J. Am. Chem. Soc.* **2005**, *127*, 11115.
- (19) Schütz, M.; Brdarski, S.; Widmark, P.-O.; Lindh, R.; Karlström, G. *J. Chem. Phys.* **1997**, *107*, 4597.
- (20) van Duijneveldt, J. B. C. M.; van Duijneveldt, F. B. *Acc. Chem. Res.* **1996**, *29*, 536.
- (21) Sprik, M.; Hutter, J.; Parrinello, M. *J. Chem. Phys.* **1996**, *105*, 1142.
- (22) Marx, D.; Tuckerman, M. E.; Hutter, J.; Parrinello, M. *Nature* **1999**, *397*, 601.
- (23) Tuckerman, M. E.; Marx, D.; Parrinello, M. *Nature* **2002**, *417*, 925.
- (24) Iuchi, S.; Morita, A.; Kato, S. *J. Phys. Chem. B* **2002**, *196*, 3466.
- (25) Yu, H.; Hansson, T.; van Gunsteren, W. F. *J. Chem. Phys.* **2003**, *118*, 221.
- (26) Silvestrelli, P. L.; Bernasconi, M.; Parrinello, M. *Chem. Phys. Lett.* **1997**, *277*, 478.
- (27) Malaspina, T.; Coutinho, K.; Canuto, S. *J. Chem. Phys.* **2002**, *117*, 1692.
- (28) Pagliai, M.; Bellucci, L.; Muniz-Miranda, M.; Cardini, G.; Schettino, V. *Phys. Chem. Chem. Phys.* **2006**, *8*, 171.
- (29) Maes, G.; Smets, J.; Adamowicz, L.; McCarthy, W.; Van Bael, M. K.; Houben, L.; Schoone, K. *J. Mol. Struct.* **1997**, *410–411*, 315.
- (30) Van Bael, M. K.; Smets, J.; Schoone, K.; Houben, L.; McCarthy, W.; Adamowicz, L.; Nowak, M. J.; Maes, G. *J. Phys. Chem. A* **1997**, *101*, 2397.
- (31) Smets, J.; McCarthy, W.; Maes, G.; Adamowicz, L. *J. Mol. Struct.* **1999**, *476*, 27.
- (32) Dkhissi, A.; Adamowicz, L.; Maes, G. *J. Phys. Chem. A* **2000**, *104*, 2112.
- (33) Schoone, K.; Smets, J.; Ramaekers, R.; Houben, L.; Adamowicz, L.; Maes, G. *J. Mol. Struct.* **2003**, *649*, 61.
- (34) Bondarev, A. F.; Mardaeva, A. I. *Opt. Spectrosc.* **1973**, *35*, 167.